P-glycoprotein Structures Reveal Asymmetric ATP Binding and a Mechanism of Substrate Polyspecificity

Lothar Esser[1]*, Fei Zhou[1]*, Kristen M. Pluchino[1], Joseph Shiloach[2], Jichun Ma[1], Wai-kwan Tang[1], Camilo Gutierrez[1], Alexander Zhang[1], Suneet Shukla[1], James P. Madigan[1], Tongqing Zhou[3], Peter Kwong[3], Suresh V. Ambudkar[1], Michael M. Gottesman[1], and Di Xia[1#]

Supplemental Information

Supplemental Tables

Table S1. Rms deviations (Å) from global structure alignments among various P-gp variants.

	4M1M[a]	$^{\Delta lnk}$*m*P-gp	$^{\Delta lnk}$*m*P-gp +Hg	$^{\Delta lnk}$*m*P-gp +ATP	4Q9H[b]	^{FL}*m*P-gp^{Me}	^{FL}*m*P-gp	4F4C[c]
4M1M	3.34[d]	0.92[e]	0.97	0.91	6.14	6.19	1.28	4.00[h]
$^{\Delta lnk}$*m*P-gp	3.01[f]	2.76	0.93	0.76	5.76	5.80	1.23	4.30[h]
$^{\Delta lnk}$*m*P-gp Hg	3.25	3.18	3.43	0.75[a]	6.35	6.40	1.31	4.32[h]
$^{\Delta lnk}$*m*P-gp +ATP	2.98	2.80	3.20	2.84	6.28	6.34	1.23	3.30[h]
4Q9H[g]	N/A	N/A	N/A	N/A	N/A[i]	1.08	5.26	2.32[h]
^{FL}*m*P-gp$^{Me(g)}$	N/A	N/A	N/A	N/A	N/A	N/A	5.32	2.29[h]
^{FL}*m*P-gp	2.81	2.81	2.39	2.81	N/A	N/A	2.52	3.84[h]
4F4C[g]	N/A	N/A	N/A	N/A	N/A	N/A	N/A	N/A

a – Coordinates from mP-gp with bound mercury (1).
b – Coordinates from fully methylated mP-gp (2).
c – Coordinates from *C. elegance* P-gp (3).
d - Numbers in the diagonal are the superposition of two independent molecules (chain B to chain A from residues 40 to 1269) within the same crystallographic asymmetric unit of the same crystal, using lsq in Coot.
e – Numbers in the upper triangle are the superposition of molecules chain A of one crystal to chain A of another crystal (residues 40 to 1269), using lsq in Coot and CA atoms only.
f – Numbers in the lower triangle are the superposition of molecules chain A of one crystal to chain B of another (residues 40 to 1269), using lsq in Coot and CA atoms only.
g – These structures have one molecule per asymmetric unit.
h – alignments are done with molecule A if applicable using SSM in Coot.
i – Structure alignment is not applicable.

Table S2. Rms deviations (Å) of superposed NBDs of P-gp variants from different crystals

		$^{\Delta lnk}$*m*P-gp (A)		$^{\Delta lnk}$*m*P-gp (B)		^{FL}*m*P-gp^{Me}		^{FL}*m*P-gp (A)		^{FL}*m*P-gp (B)	
		NBD1[a]	**NBD2**[b]	**NBD1**	**NBD2**	**NBD1**	**NBD2**	**NBD1**	**NBD2**	**NBD1**	**NBD2**
$^{\Delta lnk}$***m*P-gp (A)**	**NBD1**	-	0.97	0.32	0.94	0.72	0.92	0.40	0.97	0.47	1.04
	NBD2		-	0.93	0.46	1.18	0.76	0.99	0.51	0.99	0.86
$^{\Delta lnk}$***m*P-gp (B)**	**NBD1**			-	0.94	0.75	0.91	0.48	0.92	0.39	1.02
	NBD2				-	1.17	0.80	1.00	0.65	1.02	0.80
^{FL}***m*P-gp^{Me}**	**NBD1**					-	1.08	0.87	1.20	0.79	1.15
	NBD2						-	1.03	0.80	0.95	0.84
^{FL}***m*P-gp (A)**	**NBD1**							-	1.07	0.38	1.06
	NBD2								-	0.97	0.82
^{FL}***m*P-gp (B)**	**NBD1**									-	1.06
	NBD2										-

a –NBD1 fragment in the residue range 387 to 620 was used for alignment, using SSM in Coot.
b –NBD2 fragment in the residue range 1028 to 1267 was used for alignment, using SSM in Coot

Table S3. Rms deviations (Å) of superposed helical regions of P-gp variants from different crystals

		$^{\Delta lnk}$*m*P-gp (A)		$^{\Delta lnk}$*m*P-gp (B)		^{FL}*m*P-gp^{Me}		^{FL}*m*P-gp (A)		^{FL}*m*P-gp (B)	
		HR1[a]	HR2[b]	HR1	HR2	HR1	HR2	HR1	HR2	HR1	HR2
$^{\Delta lnk}$*m*P-gp (A)	HR1	-	2.10	0.55	2.16	0.95	2.62	0.42	2.04	0.57	2.18
	HR2		-	2.09	0.85	2.19	1.69	2.23	0.28	2.10	0.77
$^{\Delta lnk}$*m*P-gp (B)	HR1			-	2.12	1.04	2.42	0.58	2.12	0.35	2.04
	HR2				-	2.21	1.42	2.26	0.87	2.15	0.35
^{FL}*m*P-gp^{Me}	HR1					-	4.04	0.89	4.99	1.04	4.77
	HR2						-	2.60	1.67	2.54	1.48
^{FL}*m*P-gp (A)	HR1							-	2.22	0.53	2.18
	HR2								-	2.14	0.80
^{FL}*m*P-gp (B)	HR1									-	2.15
	HR2										-

a – HR1 is defined by the residues in the range 30-206, 320-379, and 850-964.
b – HR2 is defined by the residues in the range 692-849, 965-1019, and 207-319.

Table S4. Rms deviations of different domains in the helical regions based on aligning NBDs of *m*Pgp variants to that of chain A of $^{\Delta lnk}$*m*P-gp.

Alignment of NBD1				
	NBD1[a]	**ICD1[b]**	**TMD1[c]**	**ECD1[d]**
$^{\Delta lnk}$***m*P-gp (A)**	-	-	-	-
$^{\Delta lnk}$***m*P-gp (B)**	0.32	1.48	1.43	1.27
^{FL}***m*P-gp^{Me}**	0.73	1.80	2.16	4.85
4Q9H[e]	0.85	2.76	3.65	6.41

Alignment of NBD2				
	NBD2[a]	**ICD2[b]**	**TMD2[c]**	**ECD2[d]**
$^{\Delta lnk}$***m*P-gp (A)**	-	-	-	-
$^{\Delta lnk}$***m*P-gp (B)**	0.46	0.77	4.3447	5.4632
^{FL}***m*P-gp^{Me}**	0.80	0.95	8.0638	13.5347
4Q9H	0.94	1.10	8.8983	14.7904

a – NBD1 is defined by residues in the range of 387 – 620; NBD2 is defined by residues in the range of 1028-1267.

b – ICD1 include residues 140-174, 883-924, and 358-370; ICD2 consists of residues 779-820, 242-278, and 999-1014.

c – TMD1 include residues in the range of 43-79, 102-139, 175-207, 852-882, 925-963 and 326-357. TMD2 is composed of residues in the range of 702-732, 749-778, 821-850, 106-241, 279-319, and 972-998.

d - ECD1 is defined by residues 80-101, 316-325; ECD2 is defined by residues in the range of 733-748 and 965-971.

e – Coordinates obtained from fully methylated *m*P-gp (2).

Supplemental Figure Legends

Figure S1. Constructs used in preparing various wild type and mutant mouse P-gp.

Figure S2. ATPase activity of isolated mouse P-gp constructs (A) Basal ATPase activity (nmol Pi released/min/ug protein) of wild-type mP-gp in detergent and in added soy total lipid (1:1 in mg). The activity in lipids serves as 100% in all subsequent comparisons. (B) Linker mutant retains the ability of trapping ADP by vanadate. Both wild-type *m*Pgp and $^{\Delta lnk}$*m*P-gp mutant were assayed in the presence or absence of vanadate. (C) Efflux of the fluorescent P-gp substrate Calcein-AM by ^{FL}*m*P-gp. HeLa cells, which do not express P-gp, were transduced with BacMam baculovirus genetically modified to express ^{FL}*m*P-gp. Non-transduced HeLa cells (red) and virus-transduced HeLa cells were incubated with 1 μM Calcein-AM in the presence (orange) or absence (cyan) of 100 nM elacridar, a P-gp inhibitor, for 45 mins and transport of fluorescent substrates by flow cytometry was carried out. (D). Efflux of the fluorescent P-gp substrate Calcein-AM by $^{\Delta lnk}$*m*P-gp. Carried out as described in *A* but with BacMam baculovirus genetically modified to express $^{\Delta lnk}$*m*P-gp. Fluorescence intensity (RFU) correspond to the transport capacity of ^{FL}*m*P-gp and $^{\Delta lnk}$*m*P-gp. Accumulation of fluorescent substrate Calcein-AM in non-transduced Hela cells was used as control in both (C) and (D).

Figure S3. Structure determination for $^{\Delta lnk}$*m*P-gp by experimental phasing methods (A) Figure-Of-Merit (FOM) for SAD phasing as a function of resolution. The black curve represents the FOM as calculated in SHARP in a SAD run using 20 Hg atom positions. The corresponding Phasing Power for acentric reflections is shown in blue and the end point of each bin is marked with a blue rhombus. In DM, 40 cycles of molecular averaging with mask optimization, histogram matching and solvent flattening (64%) results in a resolution-dependent FOM shown in green. (B) Stereo pair: Experimental electron density for a section of *m*P-gp in the TM region, which is overlaid with an atomic model of *m*P-gp. (C) Anomalous difference Fourier map calculated at 3.8 Å resolution for the mercurial derivative (Table 1) showing anomalous peaks contoured at 5σ shown as wire cages in magenta near all cysteine residues, which are rendered as stick models in yellow and labeled. (D) Anomalous difference Fourier map for the $^{\Delta lnk}$*m*P-gp (Table 1) showing anomalous signal near some of the methionine residues. The map was contoured at 2.5σ (magenta) and 3.0σ (cyan) levels, respectively. Overlaid on this map is the structure of mP-gp in cartoon representation and corresponding methionine residues are shown as stick models and labeled.

Figure S4. Structure of $^{\Delta lnk}$*m*P-gp and comparisons (A) The two molecules of $^{\Delta lnk}$*m*P-gp in an AU, chains A and B. Chain A is colored and Chain B is in gray. (B) Superposition of the two $^{\Delta lnk}$*m*P-gp molecules in an AU. Chain A is colored magenta and Chain B is in gray. The distances (Å) between COGs of NBDs are indicated. (C) Comparison of the nucleotide-binding site in the presence and absence of ATP. Two structures were presented: one is $^{\Delta lnk}$*m*P-gp-ATP complex and another is apo $^{\Delta lnk}$*m*P-gp**.**

These two structures are superposed for the NBD1. The bound ATP is shown as stick model with surrounding functional elements color-coded and labeled. The unwinding of C427 in the P-loop (in cyan) when ATP is bound is clearly shown. (D) Crystal packing environment for ^{FL}*m*P-gp^{Me}, showing a symmetry-related molecule (blue) inserting its ECD into the opening between the two NBDs of another molecule (magenta) in crystal.

Figure S5

Supplemental Movies

Movie S1. Topographic change in the putative drug-binding surface of P-gp as a function of the opening and closing of the two halves of P-gp The morphing study was carried out between the methylated and the linker-deleted protein within 48 steps. The two halves, TMD1 (left) and TMD2 (right), are shown as molecular surfaces, as seen from the inside of the transporter.

References:

1. Li, J., Jaimes, K. F., and Aller, S. G. (2014) Refined structures of mouse P-glycoprotein. *Protein Sci* **23**, 34-46
2. Szewczyk, P., Tao, H., McGrath, A. P., Villaluz, M., Rees, S. D., Lee, S. C., Doshi, R., Urbatsch, I. L., Zhang, Q., and Chang, G. (2015) Snapshots of ligand entry, malleable binding and induced helical movement in P-glycoprotein. *Acta Crystallogr D Biol Crystallogr* **71**, 732-741
3. Jin, M., Oldham, M. L., Zhang, Q., and Chen, J. (2012) Crystal structure of the multidrug transporter P-glycoprotein from Caenorhabditis elegans. *Nature* **490**, 566-569

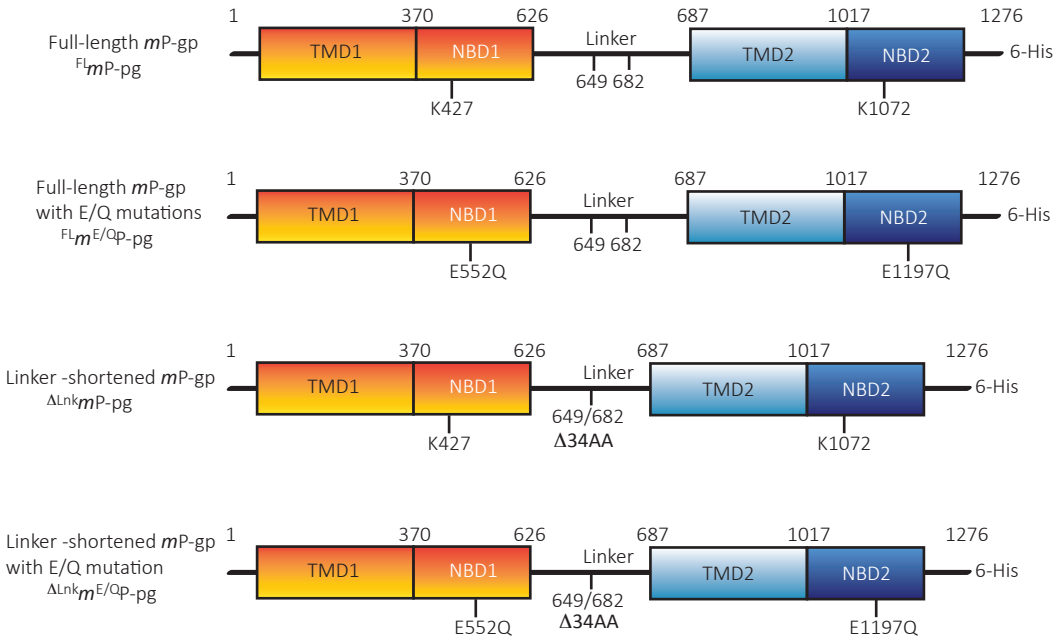

Esser, Zhou et al., Figure S1

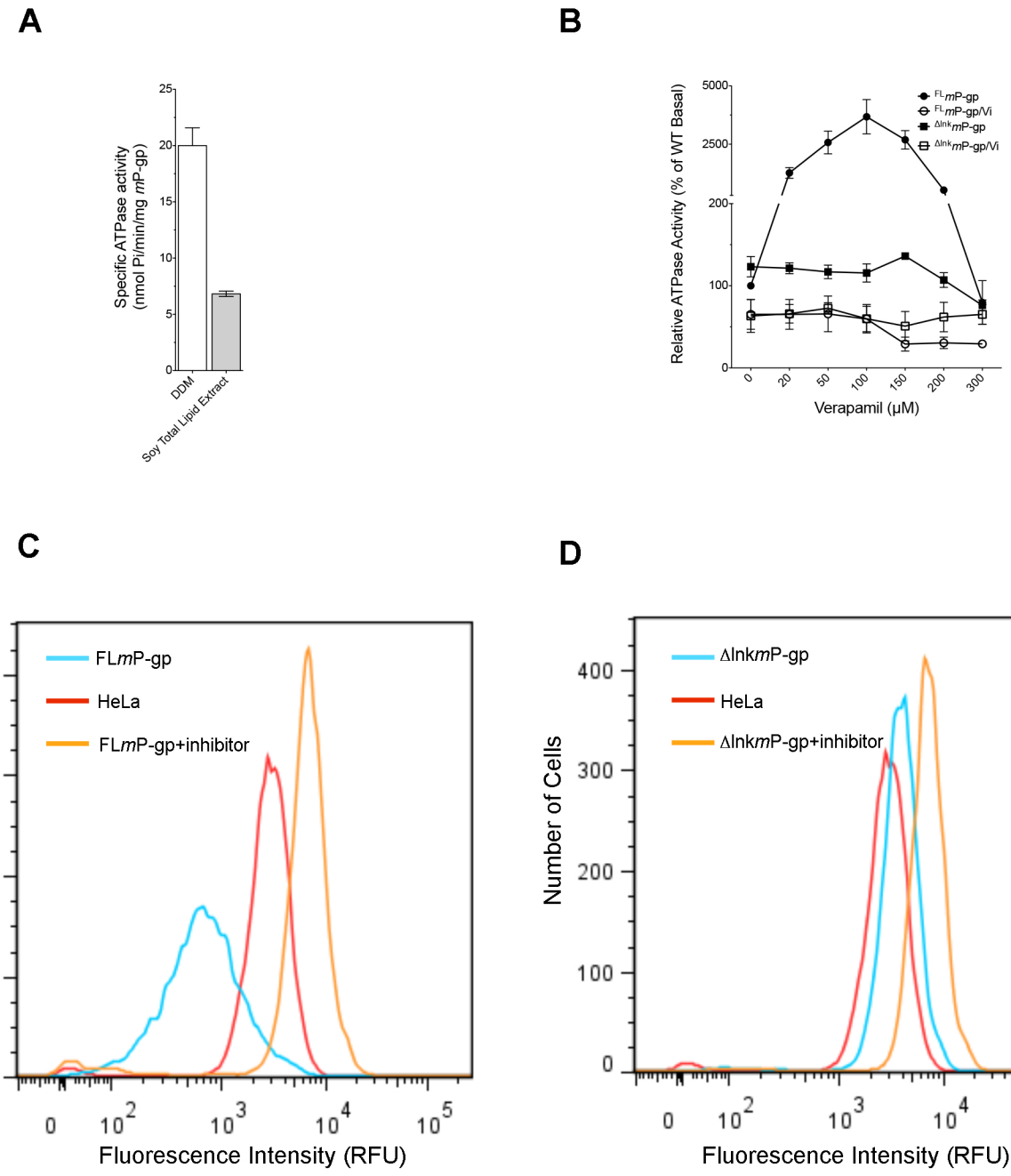

Esser, Zhou et al., Figure S2

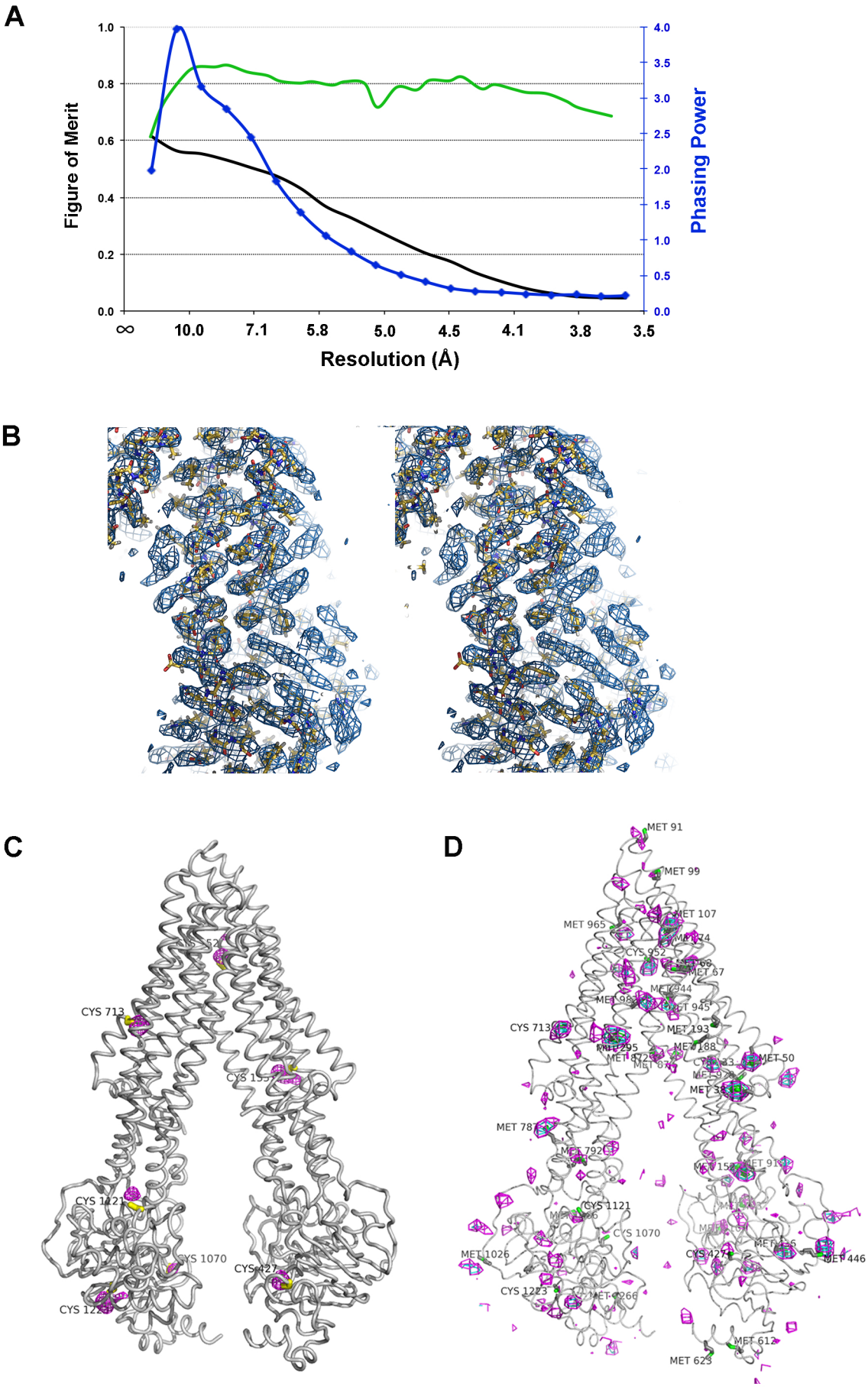

Esser, Zhou et al., Figure S3

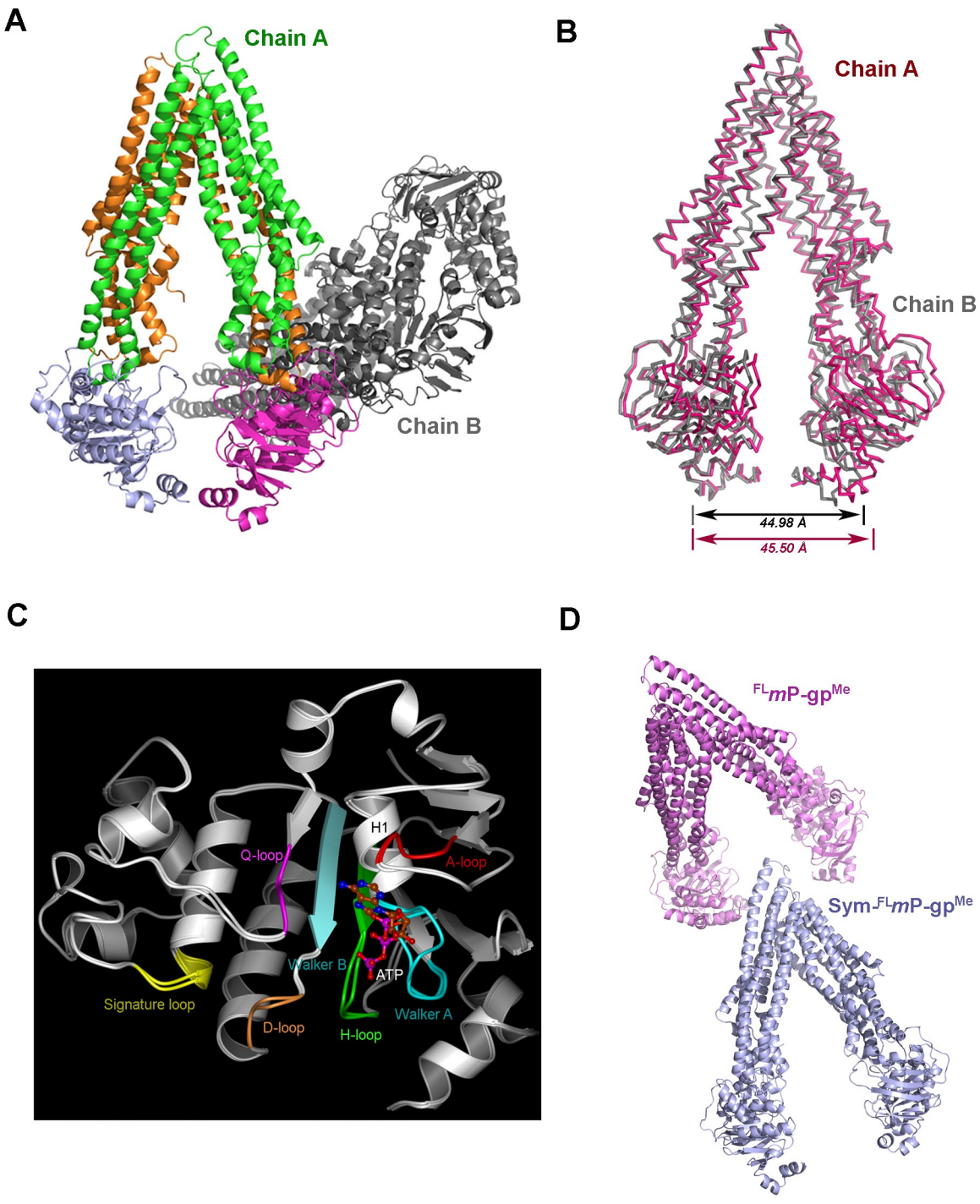

Esser, Zhou et al., Figure S4